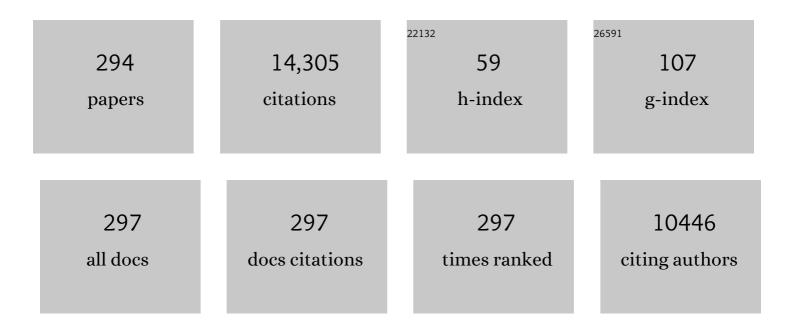


List of Publications by Year in descending order

Source: https://exaly.com/author-pdf/8115725/publications.pdf Version: 2024-02-01



Ãogenic Maide

#	Article	IF	CITATIONS
1	Quantitative X-ray tomography. International Materials Reviews, 2014, 59, 1-43.	9.4	975
2	Strong, tough and stiff bioinspired ceramics from brittle constituents. Nature Materials, 2014, 13, 508-514.	13.3	716
3	X-ray micro-tomography an attractive characterisation technique in materials science. Nuclear Instruments & Methods in Physics Research B, 2003, 200, 273-286.	0.6	390
4	In Situ Experiments with X ray Tomography: an Attractive Tool for Experimental Mechanics. Experimental Mechanics, 2010, 50, 289-305.	1.1	383
5	X-ray computed tomography. Nature Reviews Methods Primers, 2021, 1, .	11.8	305
6	Experimental study of porosity and its relation to fatigue mechanisms of model Al–Si7–Mg0.3 cast Al alloys. Materials Science & Engineering A: Structural Materials: Properties, Microstructure and Processing, 2001, 316, 115-126.	2.6	290
7	Finite element modelling of the actual structure of cellular materials determined by X-ray tomography. Acta Materialia, 2005, 53, 719-730.	3.8	282
8	Characterization of internal damage in a MMCp using X-ray synchrotron phase contrast microtomography. Acta Materialia, 1999, 47, 1613-1625.	3.8	261
9	On the Application of X-ray Microtomography in the Field of Materials Science. Advanced Engineering Materials, 2001, 3, 539.	1.6	254
10	Initiation and growth of damage in a dual-phase steel observed by X-ray microtomography. Acta Materialia, 2008, 56, 4954-4964.	3.8	244
11	Metastable and unstable cellular solidification of colloidal suspensions. Nature Materials, 2009, 8, 966-972.	13.3	201
12	X-ray tomography applied to the characterization of cellular materials. Related finite element modeling problems. Composites Science and Technology, 2003, 63, 2431-2443.	3.8	198
13	A 3D measurement procedure for internal local crack driving forces via synchrotron X-ray microtomography. Acta Materialia, 2004, 52, 1305-1317.	3.8	195
14	Nanoscale zoom tomography with hard x rays using Kirkpatrick-Baez optics. Applied Physics Letters, 2007, 90, 144104.	1.5	187
15	Advances in synchrotron radiation microtomography. Scripta Materialia, 2006, 55, 41-46.	2.6	166
16	Characterization by X-ray computed tomography of decohesion, porosity growth and coalescence in model metal matrix composites. Acta Materialia, 2001, 49, 2055-2063.	3.8	162
17	On the competition between particle fracture and particle decohesion in metal matrix composites. Acta Materialia, 2004, 52, 4517-4525.	3.8	161
18	Simulation and tomography analysis of textile composite reinforcement deformation at the mesoscopic scale. Composites Science and Technology, 2008, 68, 2433-2440.	3.8	158

#	Article	IF	CITATIONS
19	Characterization of the morphology of cellular ceramics by 3D image processing of X-ray tomography. Journal of the European Ceramic Society, 2007, 27, 1973-1981.	2.8	155
20	Visualization by X-ray tomography of void growth and coalescence leading to fracture in model materials. Acta Materialia, 2008, 56, 2919-2928.	3.8	149
21	Validation of void growth models using X-ray microtomography characterization of damage in dual phase steels. Acta Materialia, 2011, 59, 7564-7573.	3.8	148
22	Damage initiation in model metallic materials: X-ray tomography and modelling. Acta Materialia, 2004, 52, 2475-2487.	3.8	144
23	Compression behavior of lattice structures produced by selective laser melting: X-ray tomography based experimental and finite element approaches. Acta Materialia, 2018, 159, 395-407.	3.8	144
24	Hard x-ray phase imaging using simple propagation of a coherent synchrotron radiation beam. Journal Physics D: Applied Physics, 1999, 32, A145-A151.	1.3	138
25	Meso-scale FE analyses of textile composite reinforcement deformation based on X-ray computed tomography. Composite Structures, 2014, 116, 165-176.	3.1	134
26	Room-temperature ductility of Ti–6Al–4V alloy with α′ martensite microstructure. Materials Science & Engineering A: Structural Materials: Properties, Microstructure and Processing, 2011, 528, 1512-1520.	2.6	132
27	Characterization and modeling of void nucleation by interface decohesion in dual phase steels. Scripta Materialia, 2010, 63, 973-976.	2.6	131
28	3D composite reinforcement meso F.E. analyses based on X-ray computed tomography. Composite Structures, 2015, 132, 1094-1104.	3.1	127
29	Relationship between internal porosity and fracture strength of die-cast magnesium AM60B alloy. Materials Science & Engineering A: Structural Materials: Properties, Microstructure and Processing, 2005, 395, 315-322.	2.6	123
30	In situ X-ray tomography observation of inhomogeneous deformation in semi-solid aluminium alloys. Scripta Materialia, 2009, 61, 449-452.	2.6	117
31	Assessment of the fatigue crack closure phenomenon in damage-tolerant aluminium alloy byin-situhigh-resolution synchrotron X-ray microtomography. Philosophical Magazine, 2003, 83, 2429-2448.	0.7	108
32	In Situ Xâ€Ray Radiography and Tomography Observations of the Solidification of Aqueous Alumina Particle Suspensions—Part I: Initial Instants. Journal of the American Ceramic Society, 2009, 92, 2489-2496.	1.9	107
33	2D and 3D Characterization of Metal Foams Using X-ray Tomography. Advanced Engineering Materials, 2002, 4, 803-807.	1.6	100
34	Effect of strut orientation on the microstructure heterogeneities in AlSi10Mg lattices processed by selective laser melting. Scripta Materialia, 2017, 141, 32-35.	2.6	100
35	20ÂHz X-ray tomography during an in situ tensile test. International Journal of Fracture, 2016, 200, 3-12.	1.1	99
36	Influence of Particle Size on Ice Nucleation and Growth During the Iceâ€Templating Process. Journal of the American Ceramic Society, 2010, 93, 2507-2510.	1.9	98

#	Article	IF	CITATIONS
37	Experimental study of the compression behaviour of syntactic foams by in situ X-ray tomography. Acta Materialia, 2007, 55, 1667-1679.	3.8	96
38	Metallic foams: Radiative properties/comparison between different models. Journal of Quantitative Spectroscopy and Radiative Transfer, 2008, 109, 16-27.	1.1	96
39	Effect of build orientation on the fatigue properties of as-built Electron Beam Melted Ti-6Al-4V alloy. International Journal of Fatigue, 2019, 118, 65-76.	2.8	94
40	Damage quantification in aluminium alloys using in situ tensile tests in X-ray tomography. Engineering Fracture Mechanics, 2011, 78, 2679-2690.	2.0	90
41	Modeling the properties of closed-cell cellular materials from tomography images using finite shell elements. Acta Materialia, 2008, 56, 5524-5534.	3.8	88
42	In situ observation of ductile fracture using X-ray tomography technique. Acta Materialia, 2011, 59, 1995-2008.	3.8	87
43	3D quantitative image analysis of open-cell nickel foams under tension and compression loading using X-ray microtomography. Philosophical Magazine, 2005, 85, 2147-2175.	0.7	84
44	A study of fracture of unidirectional composites using in situ high-resolution synchrotron X-ray microtomography. Composites Science and Technology, 2006, 66, 1348-1353.	3.8	83
45	A Facile and Very Effective Method to Enhance the Mechanical Strength and the Cyclability of Siâ€Based Electrodes for Liâ€Ion Batteries. Advanced Energy Materials, 2018, 8, 1701787.	10.2	80
46	Ductilization of aluminium alloy 6056 by friction stir processing. Acta Materialia, 2017, 130, 121-136.	3.8	78
47	Time-lapse, three-dimensional in situ imaging of ice crystal growth in a colloidal silica suspension. Acta Materialia, 2013, 61, 2077-2086.	3.8	77
48	Analytical Modelling of the Radiative Properties of Metallic Foams: Contribution of Xâ€Ray Tomography. Advanced Engineering Materials, 2008, 10, 352-360.	1.6	76
49	Fast X-ray tomography and acoustic emission study of damage in metals during continuous tensile tests. Acta Materialia, 2007, 55, 6806-6815.	3.8	75
50	Particle redistribution and structural defect development during ice templating. Acta Materialia, 2012, 60, 4594-4603.	3.8	72
51	X-Ray Tomography Applied to the Characterization of Highly Porous Materials. Annual Review of Materials Research, 2012, 42, 163-178.	4.3	71
52	Solidification Study of Aluminum Alloys using Impulse Atomization: Part I: Heat Transfer Analysis of an Atomized Droplet. Canadian Metallurgical Quarterly, 2002, 41, 97-110.	0.4	69
53	Multiscale Morphological and Electrical Characterization of Charge Transport Limitations to the Power Performance of Positive Electrode Blends for Lithiumâ€lon Batteries. Advanced Energy Materials, 2017, 7, 1602239.	10.2	69
54	Observation of void nucleation, growth and coalescence in a model metal matrix composite using X-ray tomography. Materials Science & Engineering A: Structural Materials: Properties, Microstructure and Processing, 2008, 488, 435-445.	2.6	67

#	Article	IF	CITATIONS
55	Investigation of spacer size effect on architecture and mechanical properties of porous titanium. Materials Science & Engineering A: Structural Materials: Properties, Microstructure and Processing, 2011, 530, 633-642.	2.6	66
56	Characterization and micromechanical modelling of microstructural heterogeneity effects on ductile fracture of 6xxx aluminium alloys. Acta Materialia, 2016, 103, 558-572.	3.8	66
57	Self-Assembly of Faceted Particles Triggered by a Moving Ice Front. Langmuir, 2014, 30, 8656-8663.	1.6	65
58	Role of damage on the flow and fracture of particulate reinforced alloys and metal matrix composites. Acta Materialia, 1997, 45, 5261-5274.	3.8	61
59	<i>In Situ</i> Xâ€Ray Radiography and Tomography Observations of the Solidification of Aqueous Alumina Particles Suspensions. Part II: Steady State. Journal of the American Ceramic Society, 2009, 92, 2497-2503.	1.9	60
60	lce Shaping Properties, Similar to That of Antifreeze Proteins, of a Zirconium Acetate Complex. PLoS ONE, 2011, 6, e26474.	1.1	59
61	Characterization of ductile damage for a high carbon steel using 3D X-ray micro-tomography and mechanical tests – Application to the identification of a shear modified GTN model. Computational Materials Science, 2014, 84, 175-187.	1.4	59
62	Dynamics of the Morphological Degradation of Siâ€Based Anodes for Liâ€Ion Batteries Characterized by In Situ Synchrotron Xâ€Ray Tomography. Advanced Energy Materials, 2019, 9, 1803947.	10.2	59
63	Microtomographic study and finite element analysis of the porosity harmfulness in a cast aluminium alloy. International Journal of Fatigue, 2011, 33, 1514-1525.	2.8	56
64	Heterogenous void growth revealed by in situ 3-D X-ray microtomography using automatic cavity tracking. Acta Materialia, 2014, 63, 130-139.	3.8	56
65	Enhancing the tensile properties of EBM as-built thin parts: Effect of HIP and chemical etching. Materials Characterization, 2018, 143, 82-93.	1.9	55
66	In-situ X-ray tomographic monitoring of gypsum plaster setting. Cement and Concrete Research, 2016, 82, 107-116.	4.6	54
67	A synchrotron X-ray study of a Ti/SiCf composite during in situ straining. Acta Materialia, 2001, 49, 153-163.	3.8	53
68	The effect of fibre fractures in the bridging zone of fatigue cracked Ti–6Al–4V/SiC fibre composites. Acta Materialia, 2004, 52, 1423-1438.	3.8	49
69	Dynamics of the Freezing Front During the Solidification of a Colloidal Alumina Aqueous Suspension: <i>In Situ</i> Xâ€Ray Radiography, Tomography, and Modeling. Journal of the American Ceramic Society, 2011, 94, 3570-3578.	1.9	49
70	Onset of void coalescence in uniaxial tension studied by continuous X-ray tomography. Acta Materialia, 2013, 61, 1021-1036.	3.8	49
71	Experimental investigation of void coalescence in a dual phase steel using X-ray tomography. Acta Materialia, 2013, 61, 6821-6829.	3.8	49
72	Fast virtual histology using X-ray in-line phase tomography: application to the 3D anatomy of maize developing seeds. Plant Methods, 2015, 11, 55.	1.9	49

#	Article	IF	CITATIONS
73	Damage assessment in metallic structural materials using high resolution synchrotron X-ray tomography. Nuclear Instruments & Methods in Physics Research B, 2003, 200, 303-307.	0.6	48
74	Thermal conductivity of highly porous metal foams: Experimental and image based finite element analysis. International Journal of Heat and Mass Transfer, 2018, 122, 1-10.	2.5	48
75	Recent results on 3D characterisation of microstructure and damage of metal matrix composites and a metallic foam using X-ray tomography. Materials Science & Engineering A: Structural Materials: Properties, Microstructure and Processing, 2001, 319-321, 216-219.	2.6	47
76	Damage initiation and growth in metals. Comparison between modelling and tomography experiments. Journal of the Mechanics and Physics of Solids, 2005, 53, 2411-2434.	2.3	47
77	Damage evolution in TWIP and standard austenitic steel by means of 3D X ray tomography. Materials Science & Engineering A: Structural Materials: Properties, Microstructure and Processing, 2013, 579, 92-98.	2.6	47
78	Digital Volume Correlation Applied to Xâ€ray Tomography Images from Spherical Indentation Tests on Lightweight Gypsum. Strain, 2014, 50, 444-453.	1.4	47
79	Templated Grain Growth in Macroporous Materials. Journal of the American Ceramic Society, 2014, 97, 1736-1742.	1.9	47
80	Effect of Multiaxial Stress State on Morphology and Spatial Distribution of Voids in Deformed Semicrystalline Polymer Assessed by X-ray Tomography. Macromolecules, 2012, 45, 4658-4668.	2.2	46
81	Cellular solids studied by x-ray tomography and finite element modeling – a review. Journal of Materials Research, 2013, 28, 2191-2201.	1.2	46
82	Quantitative assessment of the impact of second phase particle arrangement on damage and fracture anisotropy. Acta Materialia, 2018, 148, 456-466.	3.8	46
83	Three-dimensional analysis of a compression test on stone wool. Acta Materialia, 2009, 57, 3310-3320.	3.8	45
84	Compressive performance and deformation mechanism of the dynamic gas injection aluminum foams. Materials Characterization, 2019, 147, 11-20.	1.9	45
85	The role of heterogeneity on the flow and fracture of two-phase materials. Materials Science & Engineering A: Structural Materials: Properties, Microstructure and Processing, 1997, 233, 145-154.	2.6	44
86	Porosity analysis of long-fiber-reinforced ceramic matrix composites using X-ray tomography. Scripta Materialia, 2009, 60, 388-390.	2.6	44
87	Deformation Behavior and Dynamic Recrystallization of Biomedical Co-Cr-W-Ni (L-605) Alloy. Metallurgical and Materials Transactions A: Physical Metallurgy and Materials Science, 2013, 44, 2819-2830.	1.1	44
88	Modelling the competition between interface debonding and particle fracture using a plastic strain dependent cohesive zone. Engineering Fracture Mechanics, 2010, 77, 705-718.	2.0	43
89	<i>In Situ</i> X-Ray Tomography Studies of Microstructural Evolution Combined with 3D Modeling. MRS Bulletin, 2008, 33, 611-619.	1.7	42
90	Influence of wall roughness and packing density on stagnant zone formation during funnel flow discharge from a silo: An X-ray imaging study. Chemical Engineering Science, 2013, 97, 210-224.	1.9	42

#	Article	IF	CITATIONS
91	A Multi-Scale Investigation of Pore Structure Impact on the Mobilization of Trapped Oil by Surfactant Injection. Transport in Porous Media, 2015, 109, 673-692.	1.2	42
92	SiC single fibre full-fragmentation during straining in a Ti–6Al–4V matrix studied by synchrotron X-rays. Acta Materialia, 2002, 50, 3177-3192.	3.8	41
93	2D and 3D Visualization of Ductile Fracture. Advanced Engineering Materials, 2006, 8, 469-472.	1.6	41
94	Two-scale study of the fracture of an aluminum foam by X-ray tomography and finite element modeling. Materials and Design, 2017, 120, 117-127.	3.3	41
95	Fatigue performances of chemically etched thin struts built by selective electron beam melting: Experiments and predictions. Materialia, 2020, 9, 100589.	1.3	41
96	Three-dimensional microtomographic study of Widmanstäten microstructures in an alpha/beta titanium alloy. Scripta Materialia, 2008, 58, 512-515.	2.6	39
97	Three-dimensional strain mapping using in situ X-ray synchrotron microtomography. Journal of Strain Analysis for Engineering Design, 2011, 46, 549-561.	1.0	39
98	3D morphological evolution of porous titanium by x-ray micro- and nano-tomography. Journal of Materials Research, 2013, 28, 2444-2452.	1.2	39
99	Effect of triaxiality on void growth and coalescence in model materials investigated by X-ray tomography. Acta Materialia, 2012, 60, 2829-2839.	3.8	38
100	Quantitative 3D characterization of intermetallic phases in an Al–Mg industrial alloy by X-ray microtomography. Scripta Materialia, 2006, 55, 123-126.	2.6	37
101	Microstructural analysis of alumina chromium composites by X-ray tomography and 3-D finite element simulation of thermal stresses. Scripta Materialia, 2003, 48, 1219-1224.	2.6	36
102	Nanovoid morphology and distribution in deformed HDPE studied by magnified synchrotron radiation holotomography. Polymer, 2014, 55, 6439-6443.	1.8	36
103	Solidification Study of Aluminum Alloys Using Impulse Atomization: Part ii. Effect of Cooling Rate on Microstructure. Canadian Metallurgical Quarterly, 2002, 41, 193-204.	0.4	35
104	Multiscale morphological characterization of process induced heterogeneities in blended positive electrodes for lithium–ion batteries. Journal of Materials Science, 2017, 52, 3576-3596.	1.7	35
105	Study of the damage mechanisms in an OSPREYâ,,¢ Al alloy-SiCp composite by scanning electron microscope in situ tensile tests. Materials Science & Engineering A: Structural Materials: Properties, Microstructure and Processing, 1995, 196, 135-144.	2.6	34
106	X-ray tomographic imaging of Ti/SiC composites. Journal of Microscopy, 2003, 209, 102-112.	0.8	34
107	Iceâ€Templating of Alumina Suspensions: Effect of Supercooling and Crystal Growth During the Initial Freezing Regime. Journal of the American Ceramic Society, 2012, 95, 799-804.	1.9	34
108	Evolution of the 3D Microstructure of a Si-Based Electrode for Li-Ion Batteries Investigated by FIB/SEM Tomography. Journal of the Electrochemical Society, 2016, 163, A1550-A1559.	1.3	34

#	Article	IF	CITATIONS
109	In situ characterization of Si-based anodes by coupling synchrotron X-ray tomography and diffraction. Nano Energy, 2019, 56, 799-812.	8.2	34
110	Damage assessment in an Al/SiC composite during monotonic tensile tests using synchrotron X-ray microtomography. Materials Science & Engineering A: Structural Materials: Properties, Microstructure and Processing, 1997, 234-236, 633-635.	2.6	33
111	Quantitative Assessment of Deformation-Induced Damage in a Semisolid Aluminum Alloy via X-ray Microtomography. Metallurgical and Materials Transactions A: Physical Metallurgy and Materials Science, 2008, 39, 2459-2469.	1.1	33
112	Mechanical behaviors of Ti–V–(Al, Sn) alloys with α′ martensite microstructure. Journal of Alloys and Compounds, 2011, 509, 2684-2692.	2.8	33
113	Quantitative estimation of volume changes of granular materials during silo flow using X-ray tomography. Chemical Engineering and Processing: Process Intensification, 2011, 50, 59-67.	1.8	33
114	Insight into the Directional Thermal Transport of Hexagonal Boron Nitride Composites. ACS Applied Materials & Interfaces, 2019, 11, 41726-41735.	4.0	33
115	I <i>n Situ</i> X-Ray Tomography Measurements of Deformation in Cellular Solids. MRS Bulletin, 2003, 28, 284-289.	1.7	32
116	Modeling the mechanical properties of optimally processed cordierite–mullite–alumina ceramic foams by X-ray computed tomography and finite element analysis. Acta Materialia, 2012, 60, 4235-4246.	3.8	32
117	Analysis of the bulk solid flow during gravitational silo emptying using X-ray and ECT tomography. Powder Technology, 2012, 224, 196-208.	2.1	32
118	Fracture behavior of robocast HA/β-TCP scaffolds studied by X-ray tomography and finite element modeling. Journal of the European Ceramic Society, 2017, 37, 1735-1745.	2.8	32
119	Lubricated compression and X-ray microtomography to analyse the rheology of a fibre-reinforced mortar. Rheologica Acta, 2010, 49, 221-235.	1.1	31
120	Resolution effect on the study of ductile damage using synchrotron X-ray tomography. Nuclear Instruments & Methods in Physics Research B, 2012, 284, 15-18.	0.6	31
121	3D morphological analysis of copper foams as current collectors for Li-ion batteries by means of X-ray tomography. Materials Science and Engineering B: Solid-State Materials for Advanced Technology, 2014, 187, 1-8.	1.7	31
122	Urban pollution of sediments: Impact on the physiology and burrowing activity of tubificid worms and consequences on biogeochemical processes. Science of the Total Environment, 2016, 568, 196-207.	3.9	31
123	A rationale for the influence of grain size on failure of magnesium alloy AZ31: An in situ X-ray microtomography study. Acta Materialia, 2020, 200, 619-631.	3.8	31
124	X-ray tomography and finite element simulation of the indentation behavior of metal foams. Materials Science & Engineering A: Structural Materials: Properties, Microstructure and Processing, 2004, 387-389, 321-325.	2.6	30
125	Simulation and tomography analysis of textile composite reinforcement deformation at the mesoscopic scale. International Journal of Material Forming, 2009, 2, 189-192.	0.9	30
126	In situ observation of syntactic foams under hydrostatic pressure using X-ray tomography. Acta Materialia, 2013, 61, 4035-4043.	3.8	30

#	Article	IF	CITATIONS
127	Three dimensional imaging of damage in structural materials using high resolution micro-tomography. Nuclear Instruments & Methods in Physics Research B, 2005, 238, 75-82.	0.6	29
128	Numerical Investigation of the Radiative Properties of Polymeric Foams from Tomographic Images. Journal of Thermophysics and Heat Transfer, 2010, 24, 647-658.	0.9	29
129	Ductile damage in aluminium alloy thin sheets: Correlation between micro-tomography observations and mechanical modeling. Materials Science & Engineering A: Structural Materials: Properties, Microstructure and Processing, 2012, 558, 217-225.	2.6	29
130	Non-destructive 3-D reconstruction of the martensitic phase in a dual-phase steel using synchrotron holotomography. Scripta Materialia, 2012, 66, 1077-1080.	2.6	29
131	Separation of nucleation and growth of voids during tensile deformation of a dual phase steel using synchrotron microtomography. Materials Science & Engineering A: Structural Materials: Properties, Microstructure and Processing, 2014, 589, 242-251.	2.6	29
132	Climateâ€Dependent Heatâ€Triggered Opening Mechanism of <i>Banksia</i> Seed Pods. Advanced Science, 2018, 5, 1700572.	5.6	29
133	Influence of the thermomechanical treatment on the microplastic behaviour of a wrought Al–Zn–Mg–Cu alloy. Acta Materialia, 2004, 52, 1653-1661.	3.8	28
134	Effect of particle clustering on the strengthening versus damage rivalry in particulate reinforced elastic plastic materials: A 3-D analysis from a self-consistent modelling. European Journal of Mechanics, A/Solids, 1999, 18, 785-804.	2.1	27
135	Iron ore sinter porosity characterisation with application of 3D X-ray tomography. Ironmaking and Steelmaking, 2010, 37, 313-319.	1.1	27
136	Three-dimensional investigation of grain orientation effects on void growth in commercially pure titanium. Materials Science & Engineering A: Structural Materials: Properties, Microstructure and Processing, 2016, 671, 221-232.	2.6	27
137	Detailed experimental validation and benchmarking of six models for longitudinal tensile failure of unidirectional composites. Composite Structures, 2022, 279, 114828.	3.1	27
138	Variability in erosion rates related to the state of landscape transience in the semiâ€arid Chilean Andes. Earth Surface Processes and Landforms, 2011, 36, 1736-1748.	1.2	26
139	Influence of cell aspect ratio on architecture and compressive strength of titanium foams. Materials Science & Engineering A: Structural Materials: Properties, Microstructure and Processing, 2011, 528, 7368-7374.	2.6	26
140	Quality control tool of electrode coating for lithium-ion batteries based on X-ray radiography. Journal of Power Sources, 2015, 298, 285-291.	4.0	26
141	Identification of the crushing behavior of brittle foam: From indentation to oedometric tests. Journal of the Mechanics and Physics of Solids, 2017, 98, 181-200.	2.3	26
142	Experimental stress state-dependent void nucleation behavior for advanced high strength steels. International Journal of Mechanical Sciences, 2020, 179, 105661.	3.6	26
143	Understanding the rapid solidification of Al-4.3Cu and Al-17Cu using X-ray tomography. Metallurgical and Materials Transactions A: Physical Metallurgy and Materials Science, 2006, 37, 249-257.	1.1	25
144	Characterization of porosity, structure, and mechanical properties of electrospun SiOC fiber mats. Journal of Materials Science, 2015, 50, 4221-4231.	1.7	25

#	Article	IF	CITATIONS
145	Fast InÂSitu X-Ray Microtomography Observations of Solidification and Semisolid Deformation of Al-Cu Alloys. Jom, 2012, 64, 83-88.	0.9	24
146	<i>In situ</i> tomographic investigation of damage development in ±45° carbon fibre reinforced laminates. Materials Science and Technology, 2015, 31, 587-593.	0.8	24
147	Effect of solution heat treatment on microstructure and damage accumulation in cast Al-Cu alloys. Journal of Alloys and Compounds, 2017, 697, 341-352.	2.8	24
148	Role of crystallographic orientation on intragranular void growth in polycrystalline FCC materials. International Journal of Plasticity, 2021, 147, 103104.	4.1	24
149	Structure and Mechanical Properties of AFS Sandwiches Studied by in-situ Compression Tests in X-ray Microtomography. Advanced Engineering Materials, 2004, 6, 411-415.	1.6	23
150	Modeling Grain Boundary Motion and Dynamic Recrystallization in Pure Metals. Metallurgical and Materials Transactions A: Physical Metallurgy and Materials Science, 2013, 44, 5861-5875.	1.1	23
151	Influence of fibre distribution and grain size on the mechanical behaviour of friction stir processed Mg–C composites. Materials Characterization, 2015, 107, 125-133.	1.9	23
152	Comparison of aluminium foams prepared by different methods using X-ray tomography. Materials Characterization, 2018, 138, 296-307.	1.9	23
153	On the influence of particle distribution and reverse loading on damage mechanisms of ductile steels. Materials Science & Engineering A: Structural Materials: Properties, Microstructure and Processing, 2008, 496, 223-233.	2.6	22
154	Experimental determination of the macroscopic fatigue properties of metal hollow sphere structures. Materials Letters, 2009, 63, 1131-1134.	1.3	22
155	The damage process in a biomedical Co–29Cr–6Mo–0.14N alloy analyzed by X-ray tomography and electron backscattered diffraction. Scripta Materialia, 2011, 64, 367-370.	2.6	22
156	CoCrMo cellular structures made by Electron Beam Melting studied by local tomography and finite element modelling. Materials Characterization, 2016, 116, 48-54.	1.9	22
157	Evolution of fibre deflection leading to kink-band formation in unidirectional glass fibre/epoxy composite under axial compression. Composites Science and Technology, 2021, 213, 108929.	3.8	22
158	Fatigue of Metal Hollow Spheres Structures. Advanced Engineering Materials, 2008, 10, 179-184.	1.6	21
159	Lightweight and stiff cellular ceramic structures by ice templating. Journal of Materials Research, 2014, 29, 175-181.	1.2	21
160	Fabrication and characterization of hardystonite-chitosan biocomposite scaffolds. Ceramics International, 2019, 45, 8804-8814.	2.3	21
161	A model for damage in a clustered particulate composite. Materials Science & Engineering A: Structural Materials: Properties, Microstructure and Processing, 1999, 262, 264-270.	2.6	20
162	Interfacial shear strength of Ti/SiC fibre composites measured by synchrotron strain measurement. Composites Part A: Applied Science and Manufacturing, 2002, 33, 1381-1385.	3.8	20

ÉRIC MAIRE

#	Article	IF	CITATIONS
163	Mechanical response and fracture dynamics of polymeric foams. Journal Physics D: Applied Physics, 2009, 42, 214001.	1.3	20
164	Damage in dual phase steels and its constituents studied by X-ray tomography. International Journal of Fracture, 2012, 174, 217-227.	1.1	20
165	Characterization by X-ray tomography of granulated alumina powder during in situ die compaction. Materials Characterization, 2013, 81, 111-123.	1.9	20
166	Mechanical properties of crumpled aluminum foils. Acta Materialia, 2014, 81, 98-110.	3.8	20
167	A clustering method for analysis of morphology of short natural fibers in composites based on X-ray microtomography. Composites Part A: Applied Science and Manufacturing, 2017, 102, 184-195.	3.8	20
168	Crack nucleation and growth in α/β titanium alloy with lamellar microstructure under uniaxial tension: 3D X-ray tomography analysis. Materials Science & Engineering A: Structural Materials: Properties, Microstructure and Processing, 2019, 747, 154-160.	2.6	20
169	Monitoring the morphological changes of Si-based electrodes by X-ray computed tomography: A 4D-multiscale approach. Nano Energy, 2020, 74, 104848.	8.2	20
170	Corrosion resistance of porous ferritic stainless steel produced by liquid metal dealloying of Incoloy 800. Corrosion Science, 2020, 166, 108468.	3.0	20
171	X-RAY TOMOGRAPHY STUDY OF ATOMIZED Al-Cu DROPLETS. Canadian Metallurgical Quarterly, 2004, 43, 273-282.	0.4	19
172	X-ray tomography and three-dimensional image analysis of epoxy-glass syntactic foams. Philosophical Transactions Series A, Mathematical, Physical, and Engineering Sciences, 2006, 364, 69-88.	1.6	19
173	Microstructure characterization by X-ray tomography and EBSD of porous FeCr produced by liquid metal dealloying. Materials Characterization, 2018, 144, 166-172.	1.9	19
174	Application of 3D X-ray tomography to investigation of structure of sinter mixture granules. Ironmaking and Steelmaking, 2009, 36, 416-420.	1.1	18
175	Multiscale Characterization of Composite Electrode Microstructures for High Density Lithium-ion Batteries Guided by the Specificities of Their Electronic and Ionic Transport Mechanisms. Journal of the Electrochemical Society, 2020, 167, 100521.	1.3	18
176	Damage studies in heterogeneous aluminium alloys using X-ray tomography. Philosophical Magazine, 2005, 85, 3191-3206.	0.7	17
177	Bulk evaluation of ductile damage development using high resolution tomography and laminography. Comptes Rendus Physique, 2012, 13, 328-336.	0.3	17
178	Mechanical Properties of Monofilament Entangled Materials. Advanced Engineering Materials, 2012, 14, 1128-1133.	1.6	17
179	Grain growth and static recrystallization kinetics in Co–20Cr–15W–10Ni (L-605) cobalt-base superalloy. Philosophical Magazine, 2014, 94, 1992-2008.	0.7	17
180	In situ 3D Synchrotron Laminography Assessment of Edge Fracture in Dual-Phase Steels: Quantitative and Numerical Analysis. Experimental Mechanics, 2016, 56, 177-195.	1.1	17

ÉRIC MAIRE

#	Article	IF	CITATIONS
181	In situ analysis of plasticity and damage nucleation in a Ti-6Al-4V alloy and laser weld. Materials Characterization, 2018, 146, 81-90.	1.9	17
182	Direct observation of the displacement field and microcracking in a glass by means of X-ray tomography during in situ Vickers indentation experiment. Acta Materialia, 2019, 179, 424-433.	3.8	17
183	Numerical investigation and experimental validation of physically based advanced GTN model for DP steels. Materials Science & Engineering A: Structural Materials: Properties, Microstructure and Processing, 2013, 569, 1-12.	2.6	16
184	Damage law identification from full field displacement measurement: Application to four-point bending test for plasterboard. European Journal of Mechanics, A/Solids, 2015, 49, 60-66.	2.1	16
185	Microstructural damage behaviour of Al foams. Acta Materialia, 2021, 208, 116739.	3.8	16
186	Processing and microstructural characterization of Al-Cu alloys produced from rapidly solidified powders. Metallurgical and Materials Transactions A: Physical Metallurgy and Materials Science, 2000, 31, 249-260.	1.1	15
187	Fast in-situ X-ray micro tomography characterisation of microstructural evolution and strain-induced damage in alloys at various temperatures. International Journal of Materials Research, 2010, 101, 1080-1088.	0.1	15
188	Interfacial stability and electrochemical behavior of Li/LiFePO4 batteries using novel soft and weakly adhesive photo-ionogel electrolytes. Journal of Power Sources, 2016, 330, 92-103.	4.0	15
189	Failure Mechanisms of Plasterboard in Nail Pull Test Determined by X-ray Microtomography and Digital Volume Correlation. Experimental Mechanics, 2016, 56, 1427-1437.	1.1	15
190	Revealing the Effect of Local Connectivity of Rigid Phases during Deformation at High Temperature of Cast AlSi12Cu4Ni(2,3)Mg Alloys. Materials, 2018, 11, 1300.	1.3	15
191	Structural and transient internal friction due to thermal expansion mismatch between matrix and reinforcement in Al–SiC particulate composite. Materials Science & Engineering A: Structural Materials: Properties, Microstructure and Processing, 2001, 313, 218-226.	2.6	14
192	A model for initiation and growth of damage in dualphase steels identified by X-ray micro-tomography. Revue De Metallurgie, 2008, 105, 102-107.	0.3	14
193	Phase Contrast Synchrotron Microtomography: Improving Noninvasive Investigations of Fossil Embryos In Ovo. Microscopy and Microanalysis, 2012, 18, 179-185.	0.2	14
194	Local Tomography Study of the Fracture of an ERG Metal Foam. Advanced Engineering Materials, 2013, 15, 767-772.	1.6	14
195	Spark plasma sintering of pure iron nanopowders by simple route. Powder Metallurgy, 2012, 55, 76-79.	0.9	13
196	Implementation of a damage evolution law for dual-phase steels in Gurson-type models. Materials and Design, 2015, 88, 1213-1222.	3.3	13
197	Homogeneous and heterogeneous rheology and flow-induced microstructures of a fresh fiber-reinforced mortar. Cement and Concrete Research, 2016, 82, 130-141.	4.6	13
198	Impact of the binder nature on the morphological change of sulfur electrodes upon cycling investigated by in situ characterization methods. Journal of Power Sources, 2020, 477, 228374.	4.0	13

#	Article	IF	CITATIONS
199	Experimental study of the effect of the anisotropy of orientation of the reinforcing particles on the tensile properties of aluminium matrix composites reinforced with α-alumina platelets. Materials Science & amp; Engineering A: Structural Materials: Properties, Microstructure and Processing, 1995, 203, 105-116.	2.6	12
200	Development of an Ultralow-Light-Level Luminescence Image Analysis System for Dynamic Measurements of Transcriptional Activity in Living and Migrating Cells. Analytical Biochemistry, 2000, 280, 118-127.	1.1	12
201	Constituent Particle Breakâ€Up During Hot Rolling of AA 5182. Advanced Engineering Materials, 2010, 12, 20-29.	1.6	12
202	Three-dimensional Analysis of an In Situ Double-torsion Test by X-ray Computed Tomography and Digital Volume Correlation. Experimental Mechanics, 2013, 53, 1265-1275.	1.1	12
203	Effect of stress triaxiality on porosity evolution in notched bars: Quantitative agreement between a recent dilatational model and X-ray tomography data. Mechanics Research Communications, 2013, 50, 77-82.	1.0	12
204	Tensile rupture of medial arterial tissue studied by X-ray micro-tomography on stained samples. Journal of the Mechanical Behavior of Biomedical Materials, 2018, 78, 362-368.	1.5	12
205	Analysis of shear stress promoting void evolution behavior in an α/β Ti alloy with fully lamellar microstructure. Materials Science & Engineering A: Structural Materials: Properties, Microstructure and Processing, 2018, 737, 27-39.	2.6	12
206	On the influence of mechanical loadings on the porosities of structural epoxy adhesives joints by means of in-situ X-ray microtomography. International Journal of Adhesion and Adhesives, 2020, 99, 102568.	1.4	12
207	Experimental investigation of porosities evolution in a bonded assembly by means of X-ray tomography. Journal of Adhesion, 2021, 97, 528-552.	1.8	12
208	Scale up of single-chamber microbial fuel cells with stainless steel 3D anode: Effect of electrode surface areas and electrode spacing. Bioresource Technology Reports, 2021, 13, 100632.	1.5	12
209	3D Characterization of the Influence of Porosity on Fatigue Properties of a Cast Al Alloy. Advanced Engineering Materials, 2011, 13, 194-198.	1.6	11
210	Structural characterization of solid foams. Comptes Rendus Physique, 2014, 15, 674-682.	0.3	11
211	Damage characterisation in aluminium matrix composites reinforced with amorphous metal inclusions. Materials Science and Technology, 2015, 31, 579-586.	0.8	11
212	Mechanical behaviour of a β-TCP ceramic with a random porosity: Study of the fracture path with X-ray tomography. Journal of the European Ceramic Society, 2016, 36, 3225-3233.	2.8	11
213	Cold-rolling influence on microstructure and mechanical properties of NiCr - Ag composites and porous NiCr obtained by liquid metal dealloying. Journal of Alloys and Compounds, 2017, 707, 251-256.	2.8	11
214	Self-diffusion of electrolyte species in model battery electrodes using Magic Angle Spinning and Pulsed Field Gradient Nuclear Magnetic Resonance. Journal of Power Sources, 2017, 362, 315-322.	4.0	10
215	Analysis of compaction in brittle foam with multiscale indentation tests. Mechanics of Materials, 2018, 118, 22-30.	1.7	10
216	Influence of tubificid worms on sediment structure, benthic biofilm and fauna in wetlands: A field enclosure experiment. Freshwater Biology, 2018, 63, 1420-1432.	1.2	10

#	Article	IF	CITATIONS
217	Micromechanical modelling of edge failure in 800ÂMPa advanced high strength steels. Journal of the Mechanics and Physics of Solids, 2020, 137, 103855.	2.3	10
218	Micro-tensile behavior of struts extracted from an aluminum foam. Materials Characterization, 2020, 166, 110456.	1.9	10
219	Tomography Imaging of Lithium Electrodeposits Using Neutron, Synchrotron X-Ray, and Laboratory X-Ray Sources: A Comparison. Frontiers in Energy Research, 2021, 9, .	1.2	10
220	Mechanical properties of unidirectional, porous polymer/ceramic composites for biomedical applications. Open Ceramics, 2021, 8, 100195.	1.0	10
221	Synchrotron X-ray study of micromechanics of Ti/SiCfcomposites with fibres containing defects introduced by laser drilling. Materials Science and Technology, 2002, 18, 1497-1503.	0.8	9
222	Application of X-ray computed micro-tomography to the study of damage and oxidation kinetics of thermostructural composites. Nuclear Instruments & Methods in Physics Research B, 2014, 324, 113-117.	0.6	9
223	Compressive deformation behavior of dendritic Mg–Ca(–Zn) alloys at high temperature. Materials Science & Engineering A: Structural Materials: Properties, Microstructure and Processing, 2019, 763, 138180.	2.6	9
224	Polymerization shrinkage of resin-based composites for dental restorations: A digital volume correlation study. Dental Materials, 2019, 35, 1654-1664.	1.6	9
225	Sulfur-Based Electrode Using a Polyelectrolyte Binder Studied via Coupled in Situ Synchrotron X-ray Diffraction and Tomography. ACS Applied Energy Materials, 2020, 3, 2422-2431.	2.5	9
226	On internal damping in metal matrix composites: Role of particle-matrix interfacial region. Scripta Materialia, 1997, 36, 189-193.	2.6	8
227	Use of numerical simulation of woven reinforcementforming at mesoscale: Influence of transversecompression on the global response. International Journal of Material Forming, 2010, 3, 699-702.	0.9	8
228	Two-Scale Tomography Based Finite Element Modeling of Plasticity and Damage in Aluminum Foams. Materials, 2018, 11, 1984.	1.3	8
229	Role of Hydrogen-Charging on Nucleation and Growth of Ductile Damage in Austenitic Stainless Steels. Materials, 2019, 12, 1426.	1.3	8
230	Study on Cell Deformation of Low Porosity Aluminum Foams under Quasiâ€Static Compression by Xâ€Ray Tomography. Advanced Engineering Materials, 2020, 22, 2000264.	1.6	8
231	Multiscale deformation processes during cold sintering of nanovaterite compacts. Acta Materialia, 2020, 189, 266-273.	3.8	8
232	Three dimensional analysis of nanoporous silicon particles for Li-ion batteries. Materials Characterization, 2017, 124, 165-170.	1.9	7
233	Ductilization of a powder metallurgy Al-17 wt pct Cu by means of channel-die compression and extrusion. Metallurgical and Materials Transactions A: Physical Metallurgy and Materials Science, 1998, 29, 2613-2620.	1.1	6
234	Computational determination of the mechanical behavior of textile composite reinforcement. Validation with x-ray tomography. International Journal of Material Forming, 2008, 1, 823-826.	0.9	6

#	Article	IF	CITATIONS
235	Imaging grain boundary grooves in hard-sphere colloidal bicrystals. Physical Review E, 2016, 94, 042604.	0.8	6
236	Experimental study of the fiber orientations in single and multi-ply continuous filament yarns. Journal of the Textile Institute, 2020, 111, 646-659.	1.0	6
237	Highlighting the role of heterogeneity on the indentation hardness of foamed gypsum. Journal of the European Ceramic Society, 2020, 40, 3795-3805.	2.8	6
238	On the effect of the curing cycle on the creation of pores in structural adhesive joints by means of X-ray microtomography. Journal of Adhesion, 2021, 97, 1073-1106.	1.8	6
239	Analyzing defects and their effects on the strength of a three-layer FSW joint by using X-ray microtomography, localized spectrum analysis, and acoustic emission. Materials Characterization, 2022, 190, 112069.	1.9	6
240	Measurement of 3-D Strain Distribution by means of High-Resolution X-ray CT Image and Tracking of Microstructural Features. Nippon Kinzoku Gakkaishi/Journal of the Japan Institute of Metals, 2007, 71, 181-186.	0.2	5
241	Damage characterization in Dual-Phase steels using X-ray tomography. Conference Proceedings of the Society for Experimental Mechanics, 2011, , 11-18.	0.3	5
242	<i>In situ</i> observation of plaster microstructure evolution during thermal loading. Fire and Materials, 2016, 40, 973-984.	0.9	5
243	Fatigue of Metal Hollow Spheres Structures. Engineering Materials, 2009, , 159-182.	0.3	5
244	Mechanical Properties of AM60B Die Castings A Review of the AUTO21 Program on Magnesium Die-Casting. , 0, , .		4
245	Simulation of Damage Percolation Within Aluminum Alloy Sheet. Journal of Engineering Materials and Technology, Transactions of the ASME, 2009, 131, .	0.8	4
246	Investigation of Ductile Damage in DP980 Steel Sheets Using Mechanical Tests and X-ray Micro-Tomography. , 2011, , .		4
247	Elaboration of Architectured Materials by Spark Plasma Sintering. Materials Science Forum, 0, 706-709, 1885-1892.	0.3	4
248	Gas permeability of Ti6Al4V foams prepared via gelcasting, experiments and modelling. Computational Materials Science, 2018, 152, 363-373.	1.4	4
249	Quantitative analysis of flow dynamics of organic granular materials inside a versatile silo model during time-lapse X-ray tomography experiments. Computers and Electronics in Agriculture, 2020, 172, 105346.	3.7	4
250	Large scale additive manufacturing of artificial stone components using binder jetting and their X-ray microtomography investigations. Open Ceramics, 2021, 7, 100162.	1.0	4
251	4D in situ monitoring of the setting of α plaster using synchrotron X-ray tomography with high spatial and temporal resolution. Construction and Building Materials, 2021, 304, 124632.	3.2	4
252	4D characterisation of void nucleation, void growth and void coalescence using advanced void tracking algorithm on in situ X-ray tomographic data. Materials Today Communications, 2022, 32, 103892.	0.9	4

#	Article	IF	CITATIONS
253	Microstructure and Mechanical Properties of α' Martensite Type Ti-V-Al Alloy after Cold- or Hot Working Process. Key Engineering Materials, 0, 436, 171-177.	0.4	3
254	Submicron Tomography Using High Energy Synchrotron Radiation. Advanced Structured Materials, 2011, , 151-170.	0.3	3
255	Stochastic characterization of textile reinforcements in composites based on X-ray microtomographic scans. Composite Structures, 2019, 224, 111031.	3.1	3
256	X Ray Tomography Study of Cellular Materials: Experiments and Modelling. IUTAM Symposium on Cellular, Molecular and Tissue Mechanics, 2009, , 35-42.	0.1	3
257	Modelling of Damage in Particulate Metal Matrix Composites. Key Engineering Materials, 1996, 127-131, 1167-1174.	0.4	2
258	Damage Investigation in Aluminium Alloys by X Ray Tomography. Materials Science Forum, 2006, 519-521, 821-827.	0.3	2
259	Microstructure-Aided Digital Volume Correlation. EPJ Web of Conferences, 2010, 6, 35002.	0.1	2
260	X-ray tomography analysis of the mechanical behaviour of reinforcements in composites. , 2011, , 565-587.		2
261	Comparison of Damage Evolution in Different Steels by Means of 3D X Ray Tomography. Steel Research International, 2015, 86, 1197-1203.	1.0	2
262	Effect of surface properties of capillary structures on the thermal behaviour of a LHP flat disk-shaped evaporator. International Journal of Thermal Sciences, 2019, 142, 163-175.	2.6	2
263	Effect of Porosity on the Fatigue Life of a Cast Al Alloy. Conference Proceedings of the Society for Experimental Mechanics, 2011, , 55-61.	0.3	2
264	Grain boundary characterization from particle coordinates. Physical Review Materials, 2021, 5, .	0.9	2
265	Al-ZrO2model composites elaboration by powder metallurgy. Revue De Metallurgie, 2002, 99, 1043-1049.	0.3	1
266	Application of the Three-Dimensional Damage Percolation Model and X-Ray Tomography for Damage Evolution Prediction in Aluminium Alloys. Materials Science Forum, 2006, 519-521, 1011-1016.	0.3	1
267	Porosity, Damage Evolution and Fracture in Die-Cast Magnesium Alloy AM60B. Advanced Materials Research, 2006, 15-17, 455-460.	0.3	1
268	Non Destructive Three Dimensional Imaging of Aluminium Alloys. Materials Science Forum, 2006, 519-521, 1367-1372.	0.3	1
269	<i>In Situ</i> X-Ray Microtomography Investigation of the Deformation Mechanisms of Al-Cu Alloys in the Semi-Solid State. Materials Science Forum, 0, 618-619, 275-278.	0.3	1
270	Nanograined Size Pure Iron Elaborated by Means of Spark Plasma Sintering. Materials Science Forum, 2010, 638-642, 1691-1696.	0.3	1

#	Article	IF	CITATIONS
271	Dynamic Recrystallization of Biomedical Co-Cr-W-Ni (L-605) Alloy. Materials Science Forum, 0, 706-709, 472-477.	0.3	1
272	Ductile Damage in Tension and Bending for DP980 Steel Sheets. Key Engineering Materials, 0, 554-557, 110-117.	0.4	1
273	Effect of viscosity on cavity growth in ductile damage. Mechanics of Materials, 2015, 89, 169-175.	1.7	1
274	Damage in a cast AlSi12Ni alloy: In situ tomography, 2D and 3D image correlation. Materialia, 2019, 8, 100475.	1.3	1
275	The importance of a variable fibre packing density in modelling the tensile behaviour of single filament yarns. Journal of the Textile Institute, 2021, 112, 733-741.	1.0	1
276	3D Anode Microbial Fuel Cell Characterization and Monitoring Coupling X-Ray Tomography and Electrochemical Impedance Spectroscopy. Journal of the Electrochemical Society, 2021, 168, 054513.	1.3	1
277	Ultra Fast Tomography: New Developments for 4D Studies in Material Science. , 0, , 203-208.		1
278	Understanding the mechanical behaviour of a high manganese TWIP steel by the means of in situ 3D X ray tomography. Conference Proceedings of the Society for Experimental Mechanics, 2011, , 27-32.	0.3	1
279	Mesoscopic Mechanical Analyses of Textile Composites: Validation with X-Ray Tomography. Lecture Notes in Applied and Computational Mechanics, 2010, , 71-78.	2.0	1
280	Ultra Fast Tomography: New Developments for 4D Studies in Material Science. , 2012, , 203-208.		1
281	Damage assessment of Al alloys using in situ tensile tests in x-ray tomography. , 2008, , .		0
282	Modelling the Mechanical and Thermal Properties of Cellular Materials from the Knowledge of their Architecture. Materials Research Society Symposia Proceedings, 2009, 1188, 150.	0.1	0
283	A Preliminary Study on Cell Wall Architecture of Titanium Foams. Materials Research Society Symposia Proceedings, 2009, 1188, 47.	0.1	0
284	Application of an Advanced GTN Model. , 2012, , .		0
285	On the Application of 3D X-Ray Microtomography for Studies in the Field of Iron Ore Sintering Technology. , 0, , .		0
286	Influence of the restored work-hardening rate on ductility studied by X-ray computed tomography. Philosophical Magazine Letters, 2013, 93, 379-386.	0.5	0
287	Analysis of Composite Reinforcement at Mesoscopic Scale from X-Ray Microtomography. Key Engineering Materials, 2014, 611-612, 316-323.	0.4	0
288	In situ observation of liquid metal dealloying and etching of porous FeCr by X-ray tomography and X-ray diffraction. Materialia, 2021, 18, 101125.	1.3	0

#	Article	IF	CITATIONS
289	Damage in the bulk of metal matrix composites during a monotonic loading. Revue De Metallurgie, 2004, 101, 637-649.	0.3	0
290	X-ray tomography analysis of the mechanical behaviour of reinforcements in composites. , 2011, , 579-599.		0
291	Three-Dimensional Investigation of Void Growth Leading to Fracture in Commercially Pure Titanium. , 0, , 61-66.		0
292	3D Multiscale Characterization of Silica Aerogels Composites. , 2014, , 29-34.		0
293	The Application of Self-Consistent Approaches to Modeling Mechanical Behaviour of Heterogeneous Two Phase Solids. , 1998, , 153-162.		0
294	<title>Image analysis applied to luminescence microscopy</title> . , 1998, , .		0